Supplemental Data

Dynamin GTPase regulation is altered by PH domain mutations found in centronuclear myopathy patients

Jon A. Kenniston and Mark A. Lemmon

SUPPLEMENTAL MATERIALS AND METHODS

Protein Purification

The PH domain from phospholipase C-δ_1 (PLC-δ_1) was expressed and purified from a pET11a vector as described (Lemmon *et al*, 1995).

Full-length dynamin protein was expressed in *E. coli* BL21 RP+ cells (Stratagene) grown in LB to OD_{600} = 0.5 at 37˚C, temperature-shifted to 18˚C for 1 hour, induced with 0.5 mM IPTG, and harvested the following morning (generally 14 hour induction). Cell pellets typically from 2 liters of cell culture were resuspended in 25 ml of ice cold Buffer A (25 mM HEPES pH 7.5, 500 mM NaCl) containing 10 mM imidazole and 1 mM PMSF. Cells were lysed by sonication, and lysates cleared by 4˚C centrifugation at 16,000 rpm in a Sorvall RC5 centrifuge for 30 minutes. 2 ml of a 50% slurry of Ni-NTA beads (Qiagen) was added to the cleared lysate, and mixed gently on a rotating platform for 1 h at 4˚C. Protein-bound beads were added to a fritted column, washed by gravity flow with 100 ml Buffer A + 10 mM imidazole, followed by 25 ml Buffer A + 50 mM imidazole, and protein was eluted with 15 ml Buffer A + 250 mM imidazole. Eluant was concentrated to 2.5 ml by centrifugation in a Millipore Amicon Ultra 50,000 MWCO, and protein was exchanged into Buffer B (25 mM HEPES pH 7.5, 200 mM NaCl, 2 mM DTT) using a PD10 column (GE Biosciences). Protein was bound to a Bio-Rad S2 cation exchange column, washed with 10x column volumes (CV) of Buffer B, and was eluted with a linear NaCl gradient in Buffer B (dynamin elutes ~ 300 mM NaCl). Pooled

dynamin-containing fractions were then concentrated and run on a Superose 6 10/300 GL gel filtration column (GE Healthcare) equilibrated with Buffer C (25 mM HEPES 7.5, 250 mM NaCl, 2% glycerol, 2 mM $MgCl_2$, and 2 mM DTT). Approximately 25% of the resulting purified dynamin has lost a portion of the C-terminal PRD domain due to proteolysis. However, this domain does not contribute to any of the biochemical properties investigated in this study. Only artificial, PRD-dependent dynamin oligomerization and subsequent GTPase activation has been reported in non-physiological conditions with no salts present (Hinshaw and Schmid, 1995; Warnock *et al*, 1996) in contrast to conditions used here. Importantly, bacterially-produced dynamin consistently exhibits a similar purification profile, basal GTPase activity (Warnock *et al*, 1997; Song *et al*, 2004), lipid binding properties (Bethoney *et al*, 2009), and lipid-mediated GTPase activity (Chappie *et al*, 2010; Tuma *et al*, 1993) to those of dynamin produced by over-expression in Sf9 cells or dynamin extracted from rat brain tissue. Bacterially-derived dynamin preparations were very consistent between batches. For instance, the modest two-fold change in basal GTPase activity between wild-type and A618T dynamin was strictly conserved for >10 individual preps each.

The dynamin dimer (ΔPRD/I690K/R399A) was produced by PCR mutagenesis of the pET15b Dyn1ba construct, and purified identically to full-length, wild-type dynamin with a few exceptions: Ni-NTA beads were washed with Buffer A + 25 mM imidazole (replacing the 50 mM imidazole wash), and Ni-NTA eluant was buffer exchanged, loaded and washed on the S2 cation exchange column using Buffer E (25 mM HEPES pH 7.5, 50 mM NaCl, 2 mM DTT). Protein eluted at approximately 150 mM NaCl during the linear salt gradient, and eluted from the Superose 6 gel filtration as a species with approximately half the estimated molecular weight of dynamin tetramers (~290 kDa) according to sizing standards.

All dynamin PH domain variants were expressed and purified as previously reported (Ferguson *et al*, 1994), except the flow-through from the DEAE resin was

diluted to 30 mM NaCl with 25 mM MES pH 6.0 and a second bulk purification step with 2 ml Fractogel^{TM} SO_3^- cation exchange resin (EMD) was used to further clear the lysate. After elution from the cation exchange column (in 200 mM NaCl), protein was concentrated (to 2.5 ml) by centrifugation in a Millipore Amicon Ultra 3,000 MWCO unit, and buffer exchanged into Buffer F (25 mm MES pH 6.0, 50 mM NaCl, 2 mM DTT) using a PD10 column. Protein was then loaded onto a Bio-Rad UNO S2 cation exchange column pre-equilibrated with Buffer F, washed with 10x CV Buffer F, and eluted with a salt gradient. PH domain containing fractions were concentrated by ultrafiltration and gel filtered on a Superose 75 column (GE Healthcare) pre-equilibrated with Buffer C.

Interestingly, the K562E PH mutant (present in the lipid binding pocket) did not bind with significant affinity to our cation exchange resins (consistent with previous observations that the binding affinity to these resins correlates with phospholipid binding affinity). We therefore modified the purification protocol such that the DEAE flow-through from the first chromatography step was diluted to 10 mM NaCl and the pH increased by adding 100 mM Tris-Cl, pH 8.8. Material was then reloaded onto a re-equilibrated DEAE sepharose column, washed with 20x CV of Buffer F (25 mM Tris-Cl pH 8.8, 10 mM NaCl, 2 mM DTT), and the mutated PH domain was eluted with Buffer F + 100 mM NaCl. Eluate was concentrated to 2.5 ml, buffer exchanged on a PD10 column, loaded onto a Bio-Rad UNO-Q6 anion exchange column pre-equilibrated with Buffer F, and eluted with a linear NaCl gradient. PH domain-containing fractions were pooled, concentrated and gel filtered as described for wild-type PH domain.

Sedimentation Velocity Ultracentrifugation

Dynamin dimer variants (11.6 μM) in Buffer D were spun at 42,000 rpm in an Optima XL-A analytical ultracentrifuge (Beckman) at 20˚C. Protein migration was monitored over a period of at least 4 hours by following absorbance at 280 nm. SEDNTERP

(http://www.analyticalultracentrifugation.com) was used to approximate buffer density (1.01519 g/ml), buffer viscosity (1.088×10^{-2} Poise), hydration estimate (0.4154 g of H_2O per g of protein), and protein partial specific volume (0.7373 ml/g). Data were fit using the c(s) method in SEDFIT with good residuals and no systematic deviations (Schuck, 2000).

Immunofluorescence Assays

Wild type and and CNM variants of dynamin 1 were overexpressed in tTA HeLa cells as described (Bethoney *et al*, 2009), and endocytosis of transferrin was monitored using protocols described by Lee *et al*, 1999.

Table SI R_g and D_{max} values derived from SAXS and *P(r)* curves of dynamin dimer variants [a]

Dynamin PH variant	R_g (Å)	D_{max} (Å)
wild-type	59.9 ± 0.6	180 ± 2
A618T	60.4 ± 1.2	181 ± 5
S619L	60.4 ± 0.5	181 ± 3

a All quoted values for R_g and D_{max} are averages derived from AutoGNOM runs for at least 14 individual scattering curves. Similar values were obtained when manual GNOM was used.

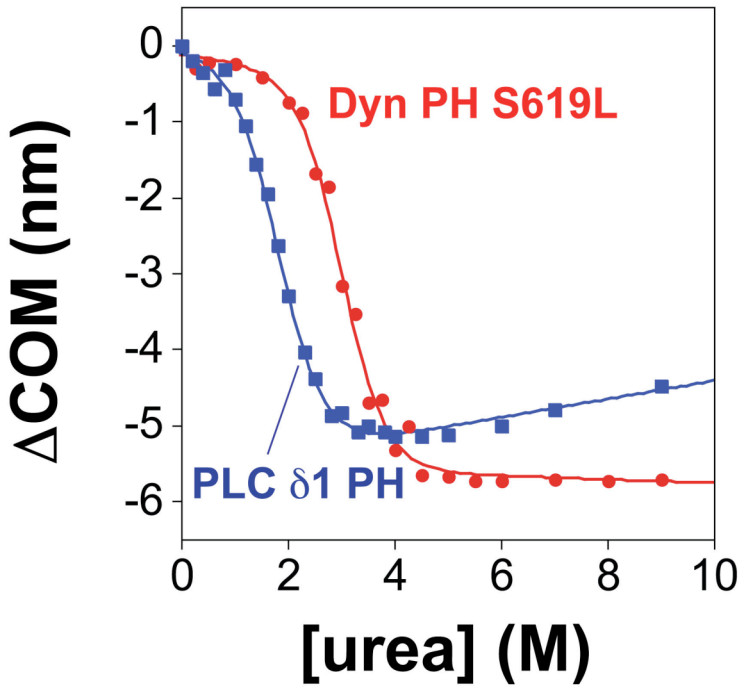

Figure S1 Urea chemical melts at 25°C of the isolated dynamin PH domain S619L variant (ΔG_u = 4.9 ± 0.5 kcal/mol: red curve) and the wild-type PH domain from PLC-δ_1 (ΔG_u = 3.2 ± 0.5 kcal/mol: blue curve). Melts comparing changes in tryptophan fluorescence center-of-mass were performed as described in the main text, except that samples were incubated at 25°C because the PLC-δ_1 PH domain is too unstable at 37°C for accurate measurement. Note that all ΔG_u values quoted in Table I were measured at 37°C.

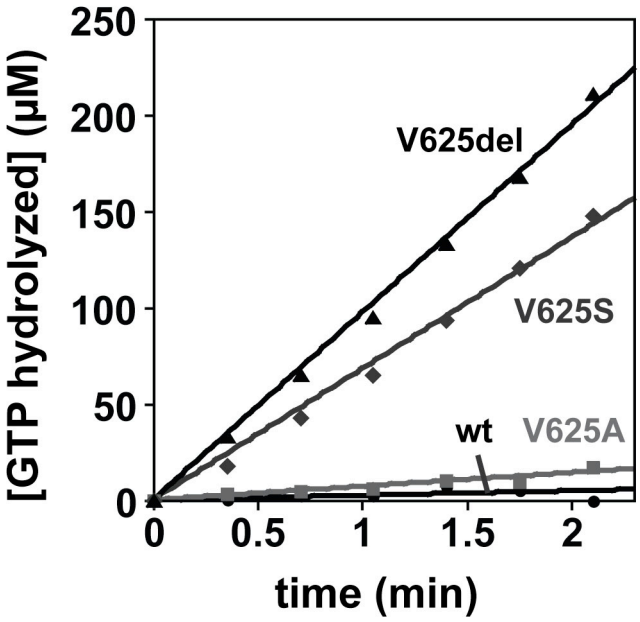

Figure S2 Basal GTP hydrolysis of the V625del, V625S, and V625A variants of intact dynamin (0.5 μM) measured in the absence of lipid using the NADH-coupled enzymatic assay (see Materials and Methods in main text). Replacing V625 with a polar residue (in V625S) leads to greatly elevated basal GTPase activity, as also seen when V625 is deleted (in V625del). By contrast, replacing V625 with a non-polar alanine residue (in V625A) results in only a mild GTPase activity increase.

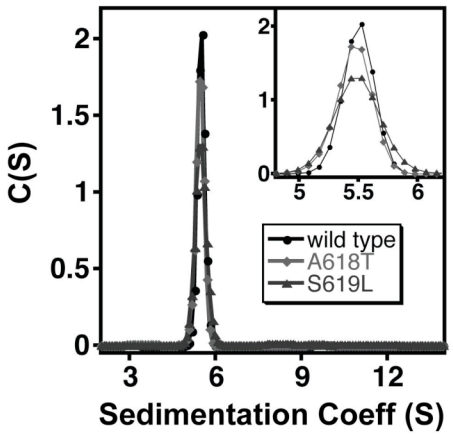

Sedimentation velocity centrifugation parameters for intact dynamin variants in the 'dimer' context			
Dynamin variant	Sedimentation Coeff (S)	Frictional Ratio f/f_0	Fit RMSD
wild-type	5.497	1.642	0.006787
A618T	5.455	1.644	0.006855
S619L	5.395	1.669	0.007437

Figure S3 Sedimentation velocity analytical ultracentrifugation of dynamin variants in the context of the "dimer" construct ΔPRD/I690K/R399A. C(S) curves (left) and best-fit hydrodynamic values (Table at right) are shown for dimer variants containing wild-type, A618T, and S619L PH domains. The sedimentation coefficients (S) of all three variants (average S = 5.48 ± 0.02) are identical to those previously reported in velocity measurements of dynamin dimer mutants (Ramachandran *et al*, 2007), and are significantly lower than values reported for tetrameric wild-type dynamin (S ≈ 12.7, data not shown and see Ramachandran *et al*, 2007). The similar frictional ratios (average f/f_0 = 1.65 ± 0.012) demonstrate that all dimer variants have a comparable, elongated shape (consistent with the tubular, elongated shape presented in Figure 6E and S6 as calculated from SAXS).

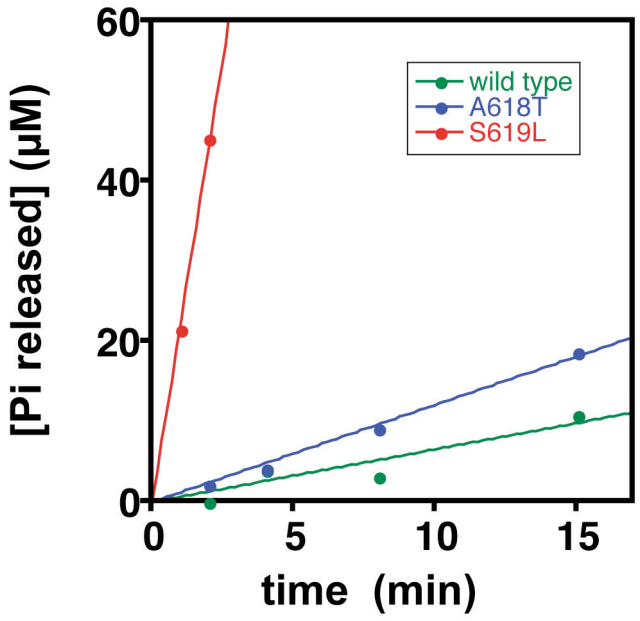

Figure S4 Basal hydrolysis of GTP (2 mM) by PH domain-mutated dynamin 'dimer' variants (0.5 μM) was monitored over time using the malachite green-based GTPase assay (see Materials and Methods in main text). CNM mutations in the C-terminal α-helix of the PH domain lead to a similar degree of basal GTPase dysregulation in the 'dimer' context as was seen in the corresponding full-length proteins. It is important to note, however, that unlike the full-length dynamin variants examined in this study, the dimer variants (including the 'wild-type') do not appear to be stable over extended periods when incubated at 37˚C. The basal GTPase rates of all dimer variants (including that with a wild-type PH domain) accelerate after ~15 min at 37˚C, resulting in a non-linear increase in P_i production when monitored over extended periods. Similarly elevated basal rates were noted for high concentrations of the related dynamin family member MxA when dimer mutations were present (Gao *et al*, 2010), possibly highlighting a common tendency for dynamin dimers to be less stable than the tetrameric forms, and consequently might self-associate into GTPase active aggregates and/or oligomers.

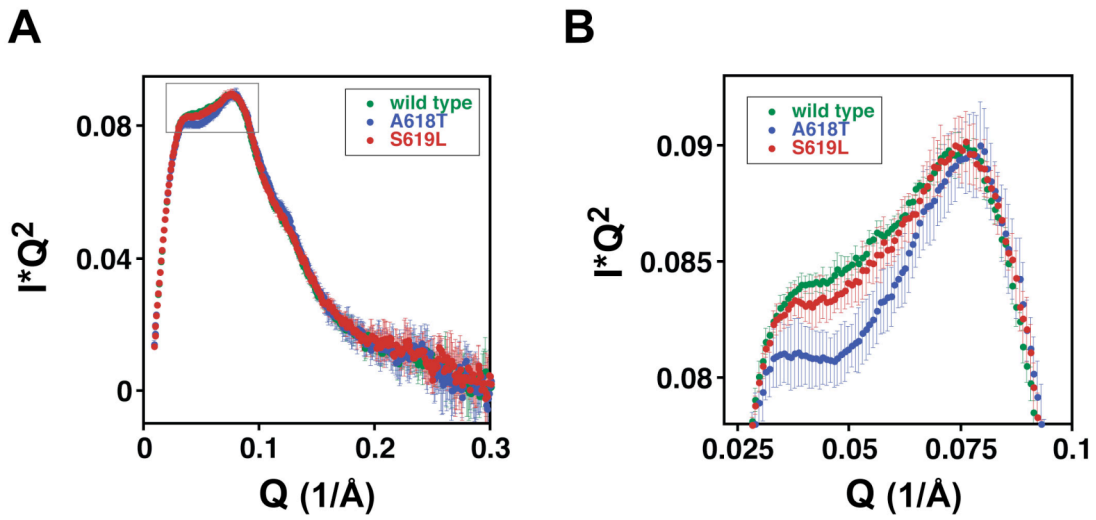

Figure S5 Conformational differences between wild-type and the A618T and S619L dimer variants are apparent when comparing primary SAXS scattering profiles. SAXS scattering curves like those presented in Figure 6A, plotted as $I*Q^2$ vs. Q (Kratky plot). The full dataset **(A)** reveals scattering differences in the low Q ranges 0.03-0.08Q and 0.1-0.13Q, indicating gross structural changes at low resolution. The boxed peak is expanded in **(B)** to highlight changes in the 0.03-0.08Q range. The data represent the average and standard deviation of 5 different individual datasets (which themselves are an average of 3 independent scattering curves).

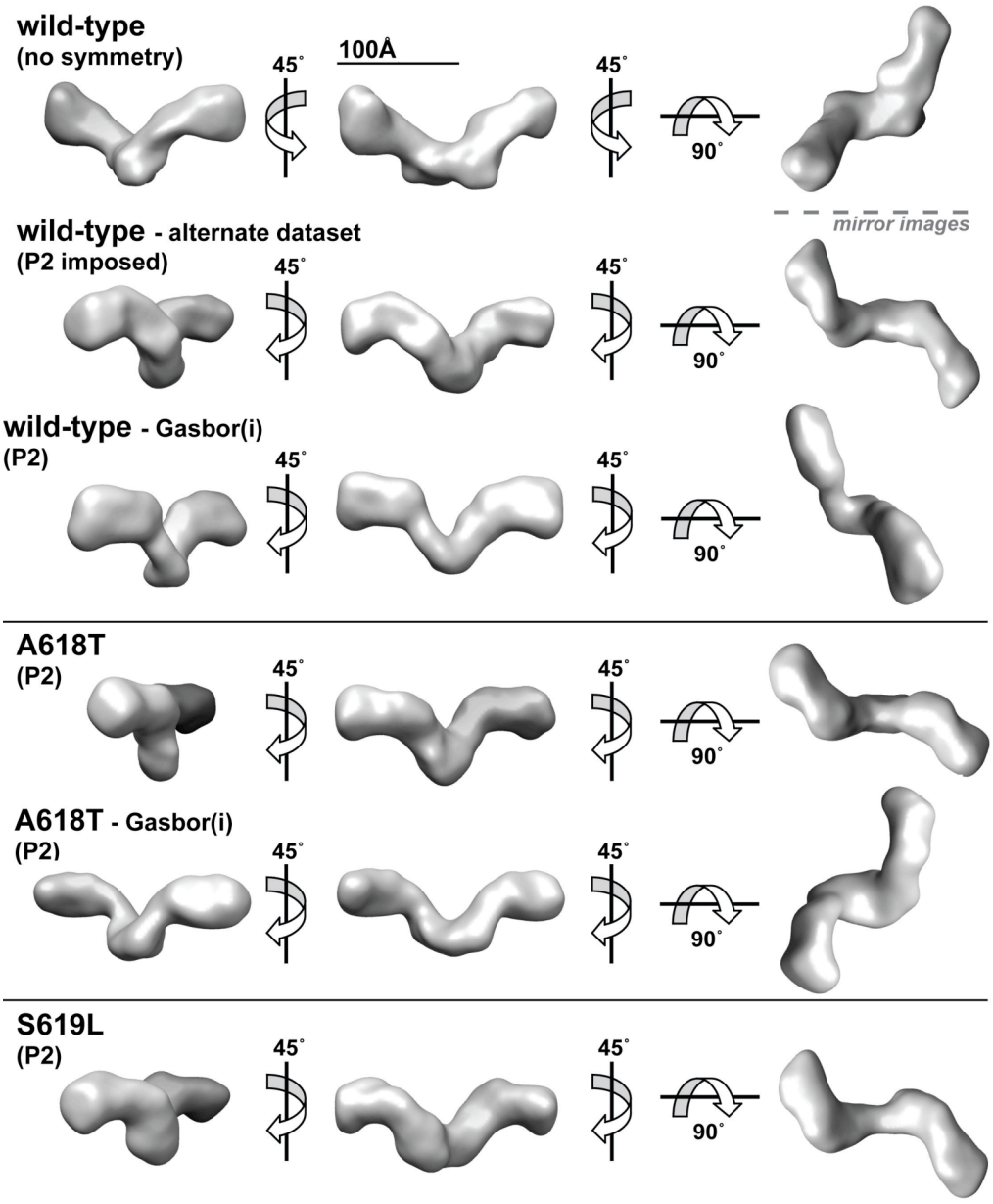

Figure S6 SAXS-based three-dimensional reconstructions of wild-type, A618T, and S619L dimer variants, using approaches reviewed by Mertens and Svergun (2010). All images were generated from most probable envelopes calculated using the Damaver suite of programs from 10 individual Dammin runs, except where noted "Gasbor(i)" which represents 10 individual shape reconstruction runs using the reciprocal space Gasbor program, followed by averaging with the Damaver suite. The dashed line (- - - -) between the two upper right envelopes is used to demonstrate that two similar, but mirror image, envelopes result from these calculations as the method does not optimize for a specific chiral species, but results in one type by chance. Different mutants, data sets, *ab initio* shape reconstruction calculations (Dammin vs Gasbor), and +/- P2 symmetry specifications all result in a similar shape. This consistency strongly points towards this envelope representing an accurate low-resolution structure of the dynamin dimer.

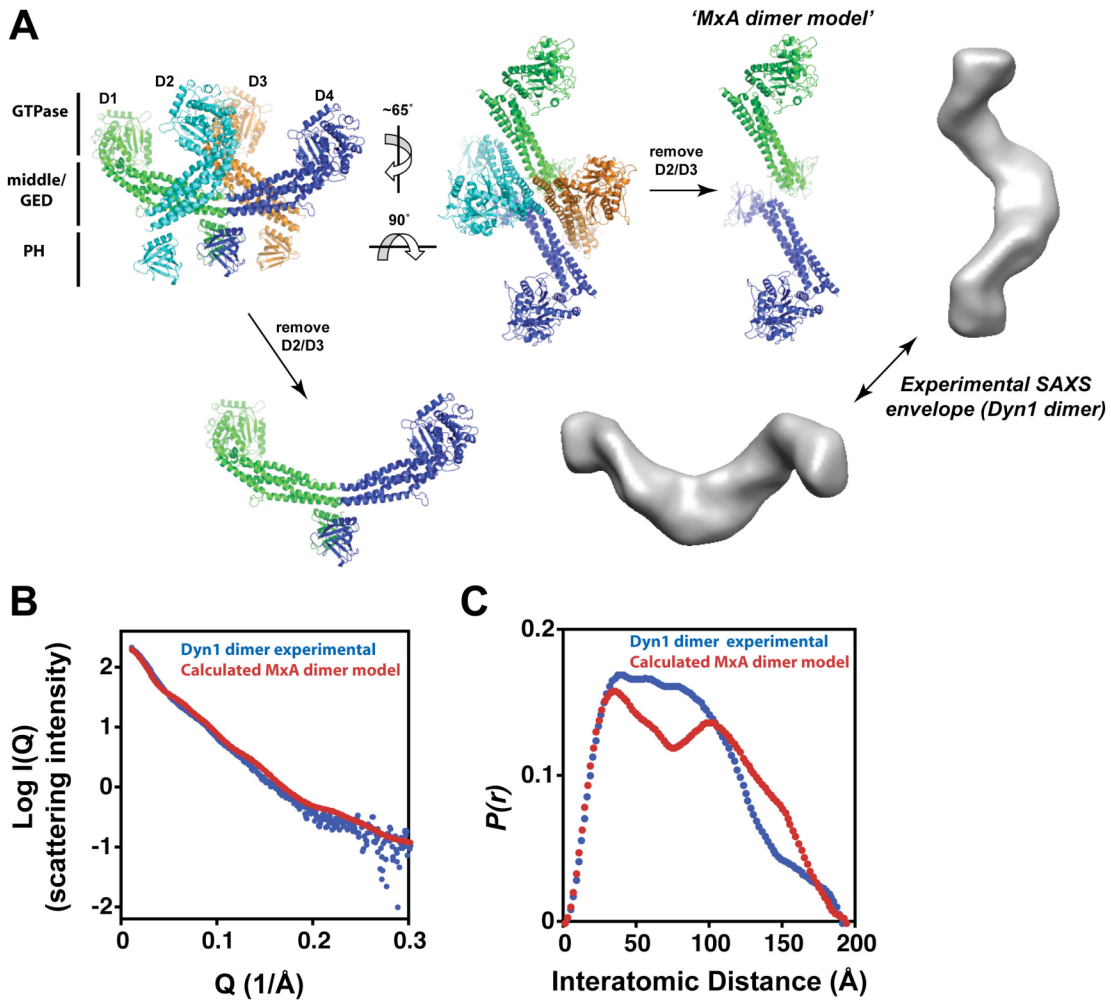

Figure S7 Comparison of the experimental SAXS envelope for a dynamin dimer with a dimer extracted from a published dynamin tetramer model. (**A**) In the dynamin tetramer model (side view shown far left) formulated by Daumke and colleagues (Gao *et al*, 2010), the four dynamin molecules are labeled D1-D4. This model was rotated (middle panel) such that the four GTPase domains are positioned nearest the viewer (and the four PH domains are furthest from the viewer). Molecules D2 and D3 (cyan and gold respectively) were then removed from the model, as expected when the R399A mutation (the dimer mutation used for dynamin SAXS constructs reported here) is present in the middle/GED 'interface 3' (Gao *et al*, 2010; Ramachandran *et al*, 2007). The resulting 'MxA dimer model' shown in the figure contains just D1 and D4, and has an overall shape that is strikingly similar to the SAXS envelopes generated in this study (shown in grey rendering – the envelope shown is the same as that in Figure S6 labeled 'wild-type alternate dataset', because this particular chiral species is most visually similar with respect to the angle of GTPase domains compared with the central middle/GED stalk). (**B**) A calculated scattering curve generated for the PDB coordinates of the 'MxA dimer model' using the program Crysol (Svergun *et al*, 1995) is reasonably similar to observed scattering curves for the dynamin dimer construct used in this study, as is (**C**) the overall shape of the resulting *P(r)* curve calculated from the hypothetical scattering curve in (B) using the program GNOM (Svergun, 1992).

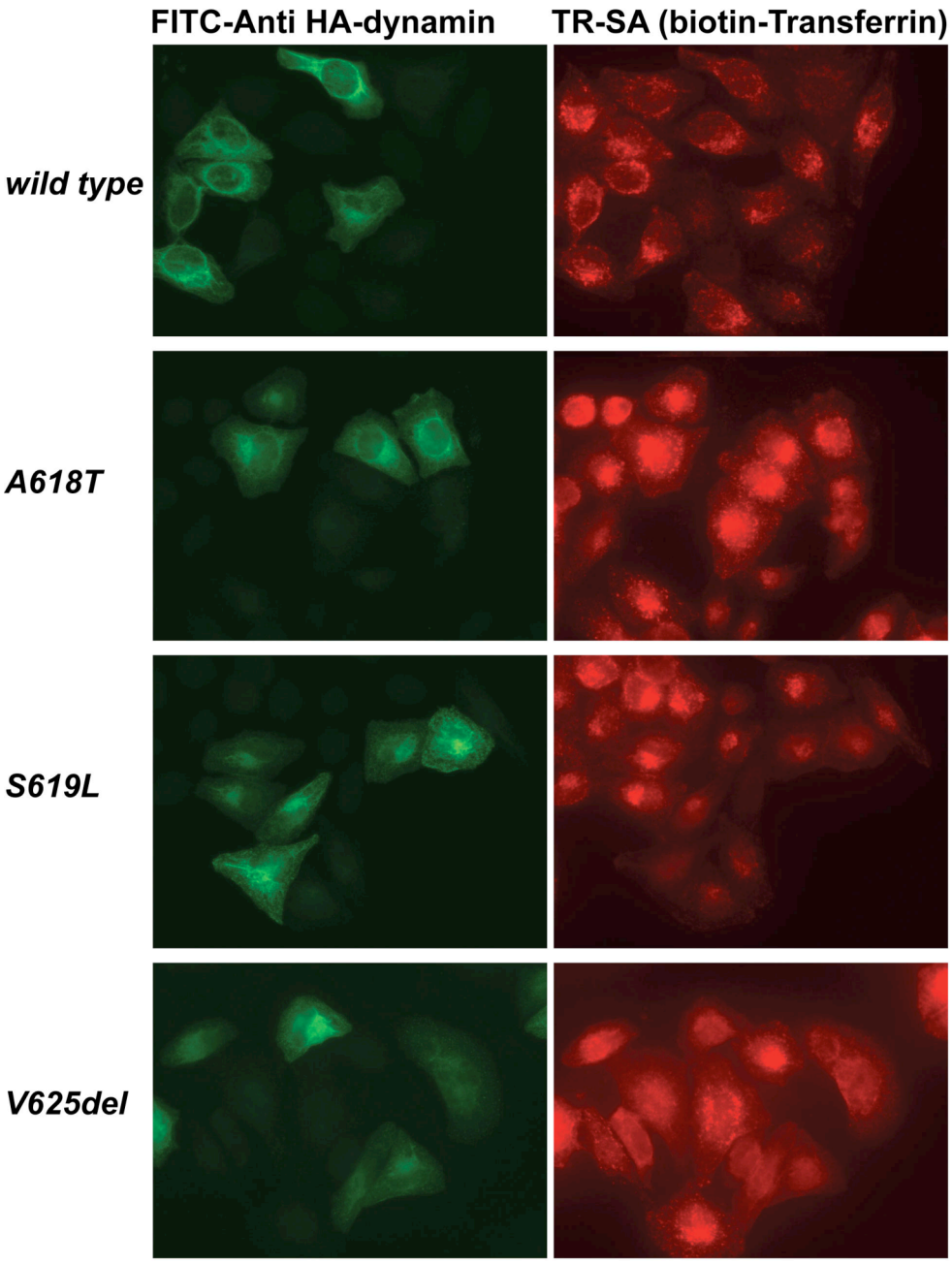

Figure S8 Transferrin endocytosis in HeLa cells overexpressing wild-type dynamin and select CNM variants. HeLa cells were transiently transfected with HA-tagged dynamin variants (green, left panels) and endocytosis of biotinylated transferrin was visualized with Texas Red-labeled streptavidin (TR-SA: red, right panels). Cells expressing wild-type or A618T dynamin exhibit a normal punctate distribution of internalized transferrin, whereas cells expressing the S619L or V625del variants exhibit evidence of dominant inhibition of endocytosis, manifest as more prominent transferrin surface staining and/or fewer internalized transferrin-positive vesicles in cells expressing the dynamin variant.

REFERENCES FOR SUPPLEMENTAL MATERIAL

Bethoney KA, King MC, Hinshaw JE, Ostap EM, Lemmon MA (2009) A possible effector role for the pleckstrin homology (PH) domain of dynamin. *Proc Natl Acad Sci USA* **106**: 13359-13364

Chappie JS, Acharya S, Leonard M, Schmid SL, Dyda F (2010) G domain dimerization controls dynamin's assembly-stimulated GTPase activity. *Nature* **465**: 435-440

Ferguson KM, Lemmon MA, Schlessinger J, Sigler PB (1994) Crystal structure at 2.2 A resolution of the pleckstrin homology domain from human dynamin. *Cell* **79**: 199-209

Gao S, von der Malsburg A, Paeschke S, Behlke J, Haller O, Kochs G, Daumke O. (2010) Structural basis of oligomerization in the stalk region of dynamin-like MxA. *Nature* **465**: 502-506

Hinshaw JE, Schmid SL (1995) Dynamin self-assembles into rings suggesting a mechanism for coated vesicle budding. *Nature* **374**: 190-192

Lee A, Frank DW, Marks MS, Lemmon MA (1999) Dominant-negative inhibition of receptor-mediated endocytosis by a dynamin-1 mutant with a defective pleckstrin homology domain. *Curr Biol* 9:261-264

Lemmon MA, Ferguson KM, O'Brien R, Sigler PB, Schlessinger J. (1995) Specific and high-affinity binding of inositol phosphates to an isolated pleckstrin homology domain. *Proc Natl Acad Sci USA* **92:**10472-10476

Mertens HD, Svergun DI (2010). Structural characterization of proteins and complexes using small-angle X-ray solution scattering. *J Struct Biol* June 15. [Epub ahead of print]

Ramachandran R, Surka M, Chappie JS, Fowler DM, Foss TR, Song BD, Schmid SL (2007) The dynamin middle domain is critical for tetramerization and higher-order self-assembly. *EMBO J* **26**: 559-566

Schuck P (2000) Size-distribution analysis of macromolecules by sedimentation velocity ultracentrifugation and lamm equation modeling. *Biophys J* **78**: 1606-1619

Song BD, Leonard M, Schmid SL (2004) Dynamin GTPase domain mutants that differentially affect GTP binding, GTP hydrolysis, and clathrin-mediated endocytosis. *J Biol Chem* **279**: 40431-40436

Svergun DI (1992) Determination of the regularization parameter in indirect-transform methods using perceptual criteria. *J Appl Cryst* **25**: 495-503

Svergun DI, Barberato C, Koch MH (1995) CRYSOL - a program to evaluate X-ray solution scattering of biological macromolecules from atomic coordinates. *J Appl Cryst* **28**: 768-773

Tuma PL, Stanchniak MC, Collins CA (1993) Activation of dynamin GTPase by acidic phospholipids and endogenous rat brain vesicles. *J Biol Chem* **268**: 17240-17246

Warnock DE, Hinshaw JE, Schmid SL (1996) Dynamin self-assembly stimulates its GTPase activity. *J Biol Chem* **271**: 22310-22314

Warnock DE, Baba T, Schmid SL (1997) Ubiquitously expressed dynamin-II has a higher intrinsic GTPase activity and a greater propensity for self-assembly than neuronal dynamin-I. *Mol Biol Cell* **8**: 2553-2562